

Experimental Review of Photon Structure Function Data

Richard Nisius

Max-Planck-Institut für Physik (Werner-Heisenberg-Institut), Föhringer Ring 6, D-80805 München, Germany, E-mail: Richard.Nisius@mpp.mpg.de*

DOI: will be assigned

The present knowledge of the structure of the photon is presented based on results obtained by measurements of photon structure functions at e^+e^- collider. Results are presented both for the QED structure of the photon as well as for the hadronic structure, where the data are also compared to recent parametrisations of the hadronic structure function $F_2^\gamma(x, Q^2)$. Prospects of future photon structure function measurements, especially at an International Linear Collider are outlined.

1 Introduction

The measurements of photon structure functions have a long tradition since the first of such measurements was performed by the PLUTO Collaboration in 1981. The investigations concern the QED structure of the photon as well as the hadronic structure. For the hadronic structure function $F_2^\gamma(x, Q^2)$ the main areas of interest are the behavior at low values of x and the evolution with the momentum scale Q^2 , which is predicted by QCD to be logarithmic. The experimental information is dominated by the results from the four LEP experiments.

This review is based on earlier work [1, 2] and as an extension provides a number of updated figures, together with a comparison of the experimental data with new parametrisations of $F_2^\gamma(x, Q^2)$ that became available since then. Only results on the structure of quasi-real photons are discussed here. The structure of virtual photons and the corresponding measurements of effective structure functions are detailed in [3].

2 Structure function measurements

The photon can fluctuate into a fermion–anti-fermion state consistent with the quantum numbers of the photon and within the limitations set by the Heisenberg uncertainty principle. These fluctuations are favored, i.e. have the longest lifetimes, for high energetic photons of low virtuality. If such a fluctuation of the photon is probed, the photon reveals its structure. Using this feature, measurements of photon structure functions are obtained from the differential cross-section of the deep-inelastic electron-photon scattering¹ process sketched in Figure 1. In this

*Invited talk presented at the Photon09 Conference in Hamburg on May 12, 2009.

¹In this paper, the term electron encompasses positrons throughout.

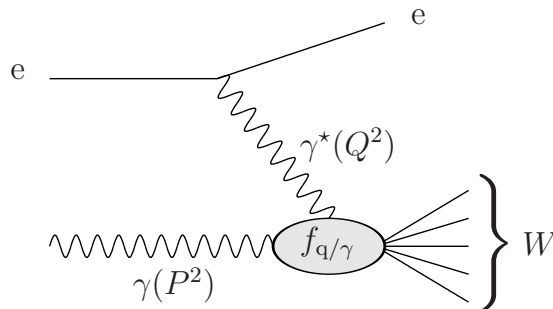


Figure 1: A sketch of the deep-inelastic electron-photon scattering process.

process the structure of the quasi-real photon, γ , radiated off an electron from one beam is probed by the virtual photon, γ^* . The γ^* is radiated off an electron from the other beam such that this electron is deflected into the detector.

The detailed formalism for the scattering of photons of arbitrary virtualities can be found in [1]. For deep-inelastic electron-photon scattering on quasi-real photons the equation reduces to the well known formula:

$$\frac{d^2\sigma_{e\gamma\rightarrow eX}}{dx dQ^2} = \frac{2\pi\alpha^2}{x Q^4} [(1 + (1 - y)^2) F_2^\gamma(x, Q^2) - y^2 F_L^\gamma(x, Q^2)] \quad \text{with: } x = \frac{Q^2}{P^2 + Q^2 + W^2}$$

The absolute values of the four momentum squared of the virtual and quasi-real photons are denoted Q^2 and P^2 , with $P^2 \ll Q^2$. The symbols x and y denote the usual dimensionless variables of deep-inelastic scattering, W denotes the invariant mass of the final state excluding the electrons, and α is the fine structure constant. The flux of the incoming photons, $f_\gamma(z, P^2)$, where z is the fraction of the electron energy carried by the photon, is usually taken from the equivalent photon approximation, EPA. At leading order, the structure function $F_2^\gamma(x, Q^2)$ is proportional to the parton content, $f_{q/\gamma}$, of the photon, and therefore reveals the structure of the photon. In the region of small y studied, $y \ll 1$, the contribution of the term containing $F_L^\gamma(x, Q^2)$ is small, and is usually neglected.

2.1 QED structure

The QED structure function $F_{2,\text{QED}}^\gamma$ of the photon is measured from deep-inelastic electron-photon scattering events in which a pair of muons is produced by the $\gamma\gamma^*$ system. Figure 2 shows the present world data on this measurement. An update is expected when the ongoing L3 analysis [4] is finalized. The data span a range of about two orders of magnitude in Q^2 and have a precision down to about 5%. With this precision, the treatment of the small but non-zero virtuality of the quasi-real photon is important, as are electroweak radiative corrections to the deep inelastically scattered electron. Unfortunately, the treatment of these corrections is different for the various experiments, see [1] for details.

In addition to the measurements of $F_{2,\text{QED}}^\gamma$ further structure functions [5] have been obtained by analyzing the azimuthal correlation between the scattering plane of the deep inelastically scattered electron and the plane spanned by the muon pair. Good agreement between data and predictions has been found. Also the scattering of two highly virtual photons has been

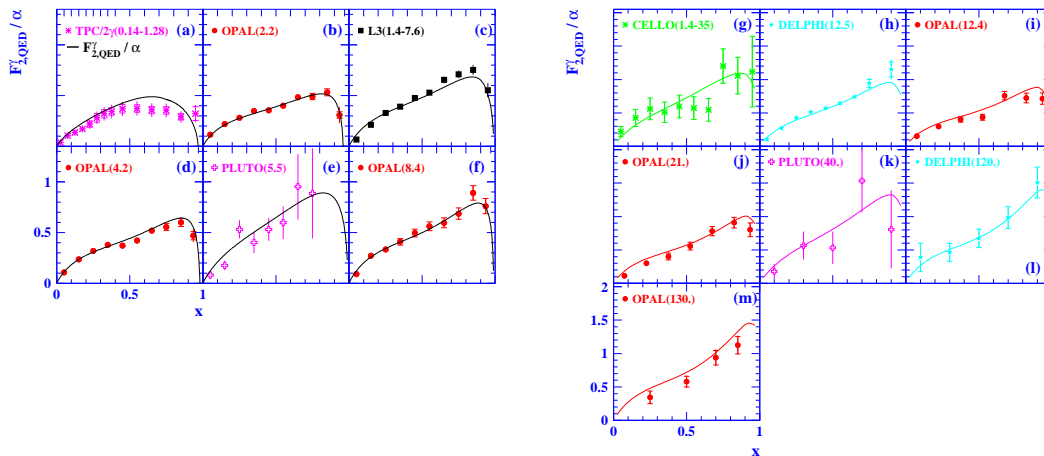


Figure 2: The world data on the QED structure function $F_{2,QED}^\gamma$ of the photon.

analyzed, and an indirect evidence for the presence of interference terms has been found [6]. Both these measurements are discussed in detail in [1].

Apart from shining light on the QED structure of the photon the determination of the QED structure functions of the photon serves two experimental purposes. It is a test bed for preparing the tools for the measurements of $F_2^\gamma(x, Q^2)$, and it sets the limit of precision that could possibly be obtained in the more complex case of hadronic final states.

2.2 Hadronic structure

The measurement of the hadronic structure of the photon is hampered by the fact that for measuring x , the invariant mass W of the hadronic final state has to be reconstructed. This is because the energy of the incoming quasi-real photon is not known, and consequently, reconstruction of x from the deep-inelastically scattered electron alone is impossible. Since the hadronic state is not perfectly described by the available Monte Carlo models, and part of the final state hadrons are scattered into the forward regions of the detectors which are only equipped with electromagnetic calorimeters, or even outside of the detector acceptance, the precision with which x can be obtained is limited, especially at large values of W and correspondingly low values of x . At large values of Q^2 the value of x is determined much more precisely, and also the data are much better described by the Monte Carlo models. The problems at low values of x are partly overcome by sophisticated unfolding techniques, and by constraining the Monte Carlo Models by utilizing combined LEP data on the hadronic final state [7]. Still the Monte Carlo description at low values of x is one of the dominant uncertainties in this measurement, such that some LEP experiments even refrained from assigning an error due to this model dependence, but published results for individual models instead.

There is one important difference between the structure function F_2^p of the proton and $F_2^\gamma(x, Q^2)$ of the photon, which originates in the different evolution equations the two have

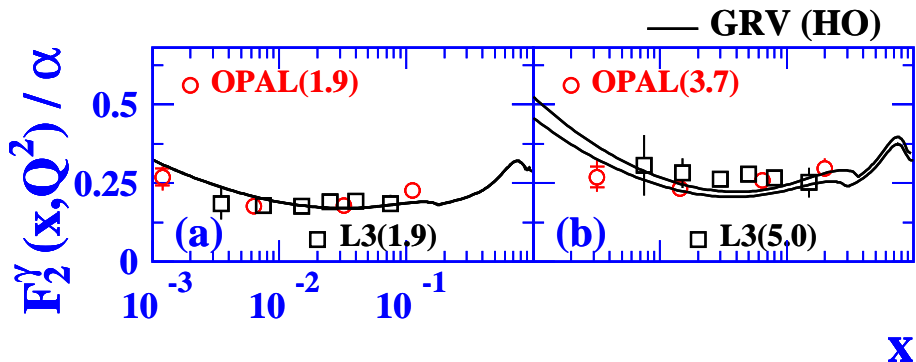


Figure 3: The world data on $F_2^\gamma(x, Q^2)$ unfolded on a logarithmic x scale.

to obey. Whereas F_2^p results from a solution of a homogeneous evolution equation, the photon structure function $F_2^\gamma(x, Q^2)$ follows an inhomogeneous evolution equation, and therefore receives two contributions. These are frequently called the hadron-like component, stemming from the general solution of the homogeneous evolution equation as for F_2^p , and the point-like component, resulting from a specific solution of the inhomogeneous evolution equation. This results in different scaling violations of F_2^p and $F_2^\gamma(x, Q^2)$.

The present status of the measurements of $F_2^\gamma(x, Q^2)$ is shown in Figures 3 and 4. Starting from the data used in [1] the TPC/ 2γ results are dropped. This is due to their unusual shape as a function of x for low values of Q^2 , and consequently very bad χ^2/dof values wrt. several parametrisations of $F_2^\gamma(x, Q^2)$, see Tables 4 and 5 in [1]. In addition, all preliminary and not yet published LEP data have been excluded, and the newly published data from ALEPH [8] and L3 [9, 10] have been added. The data span a region in Q^2 from 1.9–780 GeV² and in x from 0.0025–0.98. The experimental precision is clearly dominated by the results from the LEP experiments. There is a nice consistency between the results obtained at LEP1 energies (open symbols) with the ones from LEP2 energy data (filled symbols), which at the same Q^2 illuminate different detector parts. The higher order parametrisation from the GRV group [11], which has been obtained before many of the shown datasets became available, still gives a fair description of the data.

Since the end of LEP there has been quite some effort made in obtaining new parametrisations of $F_2^\gamma(x, Q^2)$ by several groups of authors, namely CJK [12], AFG [13] and SAL [14]. Some important ingredients of the various theoretical analyses are given below, for further details the reader is referred to the original publications.

The CJK parametrisation is based on all available $F_2^\gamma(x, Q^2)$ data for $Q^2 > 1$ GeV² including the TPC/ 2γ data and the preliminary DELPHI data taken at LEP1 energies. Various ways of treating the heavy quark, i.e. c, b , contributions are explored by the CJK group, leading to various parametrisations. The parametrisation used in this review is the CJK NLO model, which is based on the ACOT(χ) variable-flavor number scheme. For brevity, it is denoted by CJK(HO). The parametrisation is evaluated in the DIS $_\gamma$ factorization scheme, the starting scale of the evolution as obtained from the fits is $Q_0^2 = 0.765$ GeV², and the strong coupling constant, α_s , uses $\Lambda_4^{\overline{\text{MS}}} = 280$ MeV.

The AFG(HO) parametrisation is based on a subset of data, namely LEP1 data at medium

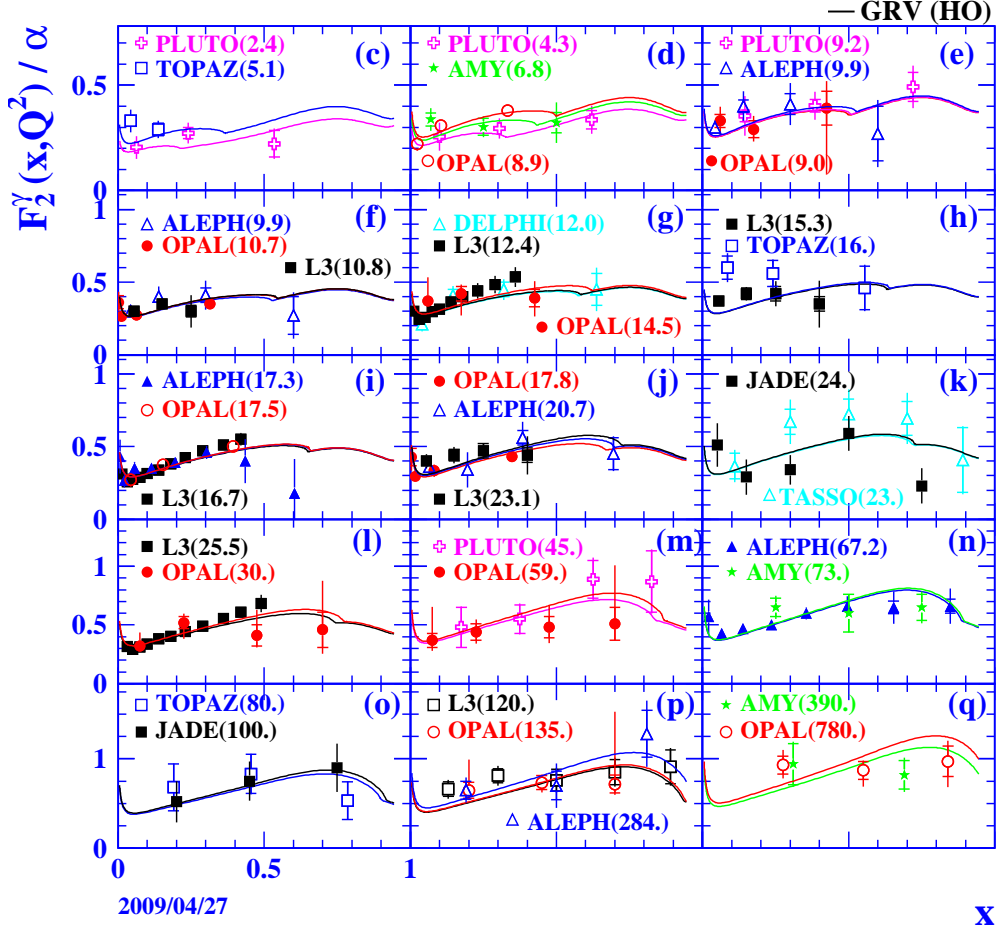


Figure 4: The world data on $F_2^\gamma(x, Q^2)$ unfolded on a linear x scale.

Q^2 , including the preliminary DELPHI data. The heavy quarks are taken to be massless, however, m_q^2/Q^2 corrections to the direct component of $F_2^\gamma(x, Q^2)$ are included in the calculation. The AFG(HO) parametrisation is evaluated in the $\overline{\text{MS}}$ factorization scheme, the starting scale for the evolution is $Q_0^2 = 0.7 \text{ GeV}^2$, again as obtained from the fit, and $\Lambda_4^{\overline{\text{MS}}} = 300 \text{ MeV}$ is used.

Finally, the SAL(HO) parametrisation is based on a completely different theoretical concept, namely the assumption of the Gribov factorization, which relates the total $\gamma\gamma$ cross-section to the total γp and pp cross-sections. At small values of x the following relation between the proton and photon structure functions is obtained: $F_2^\gamma = \frac{\sigma_{\gamma p}(W)}{\sigma_{pp}(W)} \cdot F_2^p \approx 0.43 \cdot F_2^p$, where the numerical value stems from the Donnachie-Landschoff parametrisation of the total cross-sections at large values of W . Consequently, the input data of $F_2^\gamma(x, Q^2)$ used, i.e. all published $F_2^\gamma(x, Q^2)$ data except the TPC/ 2γ data, are augmented by the ZEUS F_2^p results at $x < 0.01$

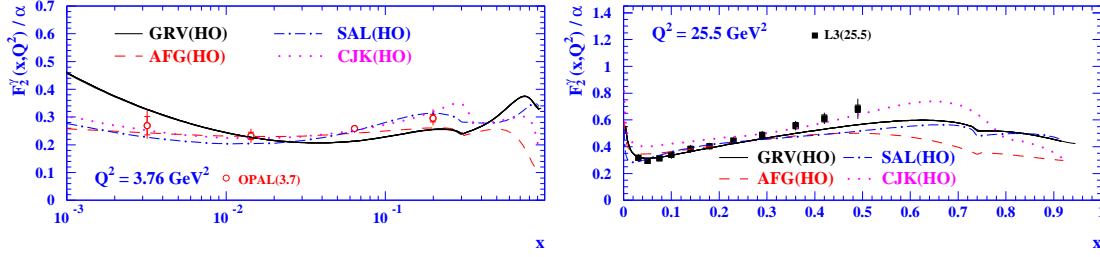


Figure 5: Parametrisations of $F_2^\gamma(x, Q^2)$ compared to LEP data at $Q^2 = 3.7$ and 25.5 GeV^2 .

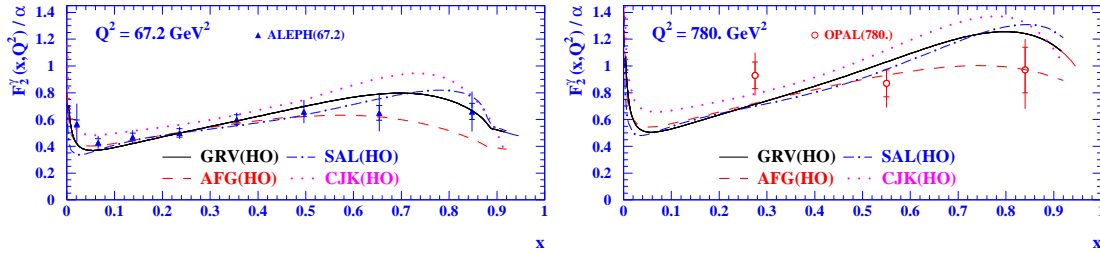


Figure 6: Parametrisations of $F_2^\gamma(x, Q^2)$ compared to LEP data at $Q^2 = 67.2$ and 780 GeV^2 .

and $Q^2 < 100 \text{ GeV}^2$. In the few overlapping regions the F_2^p data are much more precise than the corresponding $F_2^\gamma(x, Q^2)$ data. In addition the F_2^p results extend to much lower values of x . Consequently, the F_2^p data determine the low- x behavior of $F_2^\gamma(x, Q^2)$. In addition, in an attempt to better constrain the gluon distribution of the photon, also ZEUS di-jet data measured in photo-production events are used. However, it turns out that in the present kinematical region of the data the sensitivity to the gluon from the photon is rather limited. The data are strongly dominated by contributions of quarks from the photon, while the fraction of events originating from gluons from the photon is very small. The relative division of data used for the fit for $F_2^\gamma(x, Q^2)/F_2^p/\text{di-jet}$ is about 7/5/1. For the treatment of heavy quarks the SAL group derives an interpolation between the fixed flavor number scheme at low values of Q^2 and the zero-mass variable flavor number scheme at high values of Q^2 . The SAL(HO) parametrisation is evaluated in the DIS_γ factorization scheme, the starting scale of the evolution is chosen to be $Q_0^2 = 2.0 \text{ GeV}^2$, and α_s uses $\Lambda_4^{\overline{\text{MS}}} = 330 \text{ MeV}$.

Despite their rather different theoretical framework all groups face a common difficulty, they have problems fitting the preliminary DELPHI data taken at LEP1 and/or LEP2 energies. Finally, this results in an inflation of the experimental error, or even in exclusion of this data.

The fact that all parametrisations are based on different theoretical prejudice and use different experimental input to their fits makes it even more interesting to compare their behavior to the experimental data. This comparison can be seen in Figures 5 and 6 for a number of Q^2 values spanning almost the entire experimental range of the LEP data. The data shown at $Q^2 = 3.7/25.5/67.2/780 \text{ GeV}^2$ were partly used, (+), in the respective fit, and partly not, (-), where the corresponding patterns are for CJK(HO): (+/-/+/+), for AFG(HO): (+/-/-/-) and finally for SAL(HO): (+/-/+/+). Amongst the three new parametrisations CJK(HO) exhibits

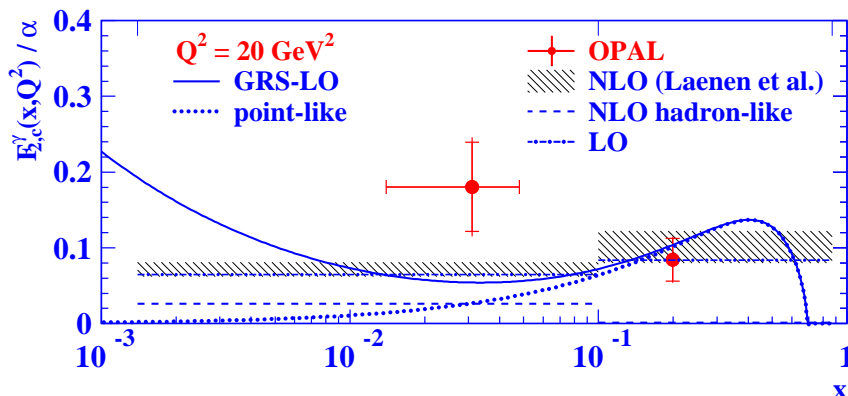


Figure 7: The measurement of $F_{2,c}^\gamma$ from OPAL.

the steepest slope at low values of x , with increasing differences to the other parametrisations for increasing Q^2 values. At medium values of x the parametrisations are closer to each other, and at high values the differences increase again, with the AFG(HO) $\overline{\text{MS}}$ parametrisation always yielding the lowest prediction. For comparison, the old GRV prediction generally lies in the middle of the new predictions, but for the lowest x values at $Q^2 = 3.7 \text{ GeV}^2$. Overall there is good agreement of the new parametrisations with the data at $Q^2 = 3.7/67.2/780 \text{ GeV}^2$ given the experimental uncertainties. The largest differences are seen for the data at $Q^2 = 25.5 \text{ GeV}^2$, which have not been used by any of the fits and which have rather small uncertainties assigned. Here the most notable difference to the data is at low values of x when compared to the CJK(HO) prediction, which is significantly higher than the data.

Not only the inclusive structure function $F_2^\gamma(x, Q^2)$ has been obtained experimentally, but also its charm component, $F_{2,c}^\gamma$, has been measured [15]. The charm part has been identified from the inclusive data by selecting charmed D mesons. The analysis makes use of the small phase space of the pion in the decay $D^* \rightarrow D^0 \pi$, which leads to a peaking structure in the distribution of the mass difference of the D^* and D^0 mesons. The result for $F_{2,c}^\gamma$ in two bins of x and unfolded to $Q^2 = 20 \text{ GeV}^2$ is shown in Figure 7 in comparison to several theoretical predictions. Shown are the purely perturbative calculations from [16, 17] at leading and next-to-leading order, NLO, and for the two data bins of x . This clearly shows that NLO corrections to $F_{2,c}^\gamma$ are small. In addition shown is the functional form of the leading order GRS [18] parametrisation for both the full $F_{2,c}^\gamma$ and the point-like part alone. The separation in x of the data has been such as to experimentally separate the point-like part, concentrated at large values of x , from the hadron-like part, dominating at low values of x , as can be seen e.g. by comparing to the GRS curves. Figure 7 demonstrates that the high x region is adequately described by the point-like NLO prediction with only α_s and the mass of the charm-quark, m_c , as free parameters. The behavior at low values of x is experimentally less well constrained. However, it can not be accommodated by the point-like part alone, e.g. as given by the GRS parametrisation, thereby suggesting a non-vanishing hadron-like part at low values of x also for $F_{2,c}^\gamma$. The uncertainty on the measurement at low values of x is relatively big, but largely dominated by statistical uncertainties (inner error bars), so a measurement of $F_{2,c}^\gamma$ by the other LEP experiments is highly desirable.

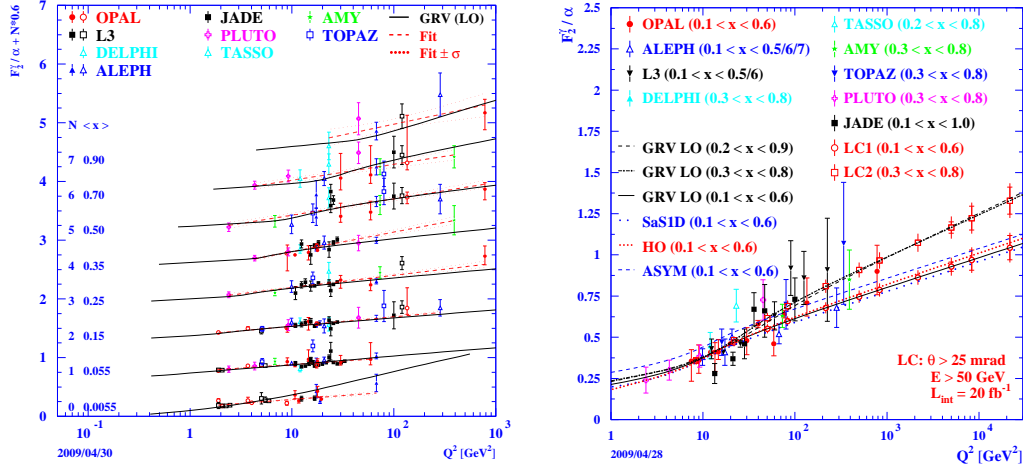


Figure 8: Positive scaling violations of $F_2^\gamma(x, Q^2)$ for various regions in x (left), and prospects for a measurement of the Q^2 evolution of $F_2^\gamma(x, Q^2)$ at an ILC (right).

One key feature of $F_2^\gamma(x, Q^2)$ is the logarithmic behavior with Q^2 as predicted by perturbative QCD. It is the point-like contribution discussed above that results in positive scaling violations of $F_2^\gamma(x, Q^2)$ for all values of x , in contrast to the proton, which exhibits negative scaling violations at high values of x , due to gluon radiation, and positive scaling violations at low values of x , due to pair creation of quark–anti-quark pairs. See [1] for a detailed assessment of this issue.

The positive scaling violations of $F_2^\gamma(x, Q^2)$ for all values of x is born out by the data as can be seen from Figure 8(left). The data are displayed as a function of Q^2 in bins of x , where each data point is shown at its nearest average x value chosen from the list on the left. In addition, for better visibility, the data points for the various bins in x are separated by constant offsets, N . Linear fits to the data of the form $F_2^\gamma(Q^2) = a + b \ln Q^2$ have been performed. The fitted values of b are significantly above zero for all bins of x , and a clear trend for increasing slope with increasing values of x is observed.

What about the future of $F_2^\gamma(x, Q^2)$ after LEP. There are two obvious candidates for future measurements, a short term opportunity is the measurement at the B-factories, where the Babar and Belle experiments are operating. The longer term option is the measurement of $F_2^\gamma(x, Q^2)$ at an International Linear Collider, ILC. The general prospects for Two-Photon physics at an ILC can be found in [19]. The higher beam energy and luminosity available at the ILC compared to LEP will allow to extend the available phase in Q^2 by about two orders in magnitude. For a detailed investigation of neutral current interactions see [20]. As an example, the measurement of the Q^2 evolution of F_2^γ at medium values of x at an e^+e^- collider is shown in Figure 8(right). At the ILC also novel features can be investigated like the measurement of the flavor decomposition of F_2^γ by exploring the exchange of W and Z bosons [21].

2.3 Summary

The measurement of photon structure functions is an interesting field of research. Unfortunately, experimentally it has come to a halt after the shut-down of LEP, since so far it has not been pursued at the B-factories and the prospects for an ILC are still uncertain.

Up to now, a wealth of data has been analyzed both in terms of the QED structure, and for the hadronic structure of the photon. In this short review only a part of the investigations could be discussed in detail. Concerning the QED structure, $F_{2,\text{QED}}^\gamma$ was investigated, as well as additional structure functions from azimuthal correlations and the interactions of two virtual photons. For the hadronic structure the emphasis is on $F_2^\gamma(x, Q^2)$ and especially its behavior at low values of x and the logarithmic scaling violations with Q^2 . In addition, the charm contribution $F_{2,c}^\gamma$ has been measured, and the interaction of two virtual photons were investigated.

I strongly hope that the future will bring us additional information from the B-factories and an ILC.

Acknowledgments

I like to thank the organizers for this interesting conference, and for giving me the opportunity to refresh my memory on this interesting field of research.

References

- [1] R. Nisius, Phys. Rep. **332** 165–317, (2000), updated figures available at:
<http://www.mppmu.mpg.de/~nisius/welcomeaux/struc.html>
- [2] R. Nisius, Nucl. Phys. B Proc. Suppl. **117** 258–261 (2003).
- [3] K. Sasaki, this conference.
- [4] K. Dehmelt, L3 Collaboration, this conference.
- [5] R. Nisius and M.H. Seymour, Phys. Lett. **B452** 409–413 (1999).
- [6] G. Abbiendi *et al.*, OPAL Collaboration, Eur. Phys. J. **C11** 409–425 (1999).
- [7] The LEP Working Group for Two-Photon Physics, ALEPH, L3 and OPAL, Eur. Phys. J. **C23** 201–223 (2002).
- [8] A. Heister *et al.*, ALEPH Collaboration, Eur. Phys. J. **C30** 145–158 (2003).
- [9] M. Acciarri *et al.*, L3 Collaboration, Phys. Lett. **B483** 373–386 (2000).
- [10] P. Achard *et al.* L3 Collaboration, Phys. Lett. **B622** 249–264 (2005).
- [11] M. Glück, E. Reya and A. Vogt, Phys. Rev. **D46** 1973–1979 (1992).
- [12] F. Cornet, P. Jankowski and M. Krawczyk, Phys. Rev. **D70** 093004 (2004).
- [13] P. Aurenche, M. Fontannaz and J.Ph. Guillet, Eur. Phys. J. **C44** 395–409 (2005).
- [14] W. Słomiński, H. Abramowicz and A. Levy, Eur. Phys. J. **C45** 633–641 (2006).
- [15] G. Abbiendi *et al.*, OPAL Collaboration, Phys. Lett. **B539** 13–24 (2002).
- [16] E. Laenen, S. Riemersma, J. Smith and W.L. van Neerven, Phys. Rev. **D49** 5753–5768 (1994).
- [17] E. Laenen and S. Riemersma, Phys. Lett. **B376** 169–176 (1996).
- [18] M. Glück, E. Reya and M. Stratmann, Phys. Rev. **D51** 3220–3229 (1995).
- [19] R. Nisius, hep-ex/9811024 (1998).
- [20] A. Vogt, Nucl. Phys. B Proc. Suppl. **82** 394–399 (2000).
- [21] A. Gehrmann-De Ridder, H. Spiesberger, and P.M. Zerwas, Phys. Lett. **B469** 259–262 (1999).